

# Variational principles in quantum Monte Carlo: the troubled story of variance minimization

Alice Cuzzocrea,<sup>1</sup> Anthony Scemama,<sup>2</sup> Wim J. Briels,<sup>1,\*</sup> Saverio Moroni,<sup>3,†</sup> and Claudia Filippi<sup>1,‡</sup>

<sup>1</sup>MESA+ Institute for Nanotechnology, University of Twente, P.O. Box 217, 7500 AE Enschede, The Netherlands

<sup>2</sup>Laboratoire de Chimie et Physique Quantiques, Université de Toulouse, CNRS, UPS, France

<sup>3</sup>CNR-IOM DEMOCRITOS, Istituto Officina dei Materiali,

and SISSA Scuola Internazionale Superiore di Studi Avanzati, Via Bonomea 265, I-34136 Trieste, Italy

We investigate the use of different variational principles in quantum Monte Carlo, namely energy and variance minimization, prompted by the interest in the robust and accurate estimate of electronic excited states. For two prototypical, challenging molecules, we readily reach the accuracy of the best available reference excitation energies using energy minimization in a state-specific or state-average fashion for states of different or equal symmetry, respectively. On the other hand, in variance minimization, where the use of suitable functionals is expected to target specific states regardless of the symmetry, we encounter severe problems for a variety of wave functions: as the variance converges, the energy drifts away from that of the selected state. This unexpected behavior is sometimes observed even when the target is the ground state, and generally prevents the robust estimate of total and excitation energies. We analyze this problem using a very simple wave function and infer that the optimization finds little or no barrier to escape from a local minimum or local plateau, eventually converging to the unique lowest-variance state instead of the target state. While the loss of the state of interest can be delayed and possibly avoided by reducing the statistical error of the gradient, for the full optimization of realistic wave functions, variance minimization with current functionals appears to be an impractical route.

## I. INTRODUCTION

Light-induced processes are at the heart of a variety of phenomena and applications which range from harnessing the response to light of biological systems to improving the technologies for renewable energies. The contribution of electronic structure theory in this field hinges on its ability to efficiently and accurately compute excited-state properties. In this context, the use of quantum Monte Carlo (QMC) methods is relatively recent and quite promising [1–9]: QMC approaches provide an accurate (stochastic) solution of the Schrödinger equation and benefit from a favorable scaling with system size and great ease of parallelization [10–12]. Importantly, recent methodological advancements [13–16] enable the fast calculation of energy derivatives and the optimization of many thousands of parameters for the internally consistent computation of QMC wave functions and geometries in the ground and excited states [9, 17].

Here, we investigate the use of two different variational principles for ground and excited states in QMC, namely, variance and energy minimization, to assess whether they allow us to fully capitalize on the increased power of minimization algorithms and availability of accurate wave functions. Variance minimization techniques [18–22] have been extensively employed in QMC for the last 30 years but their potential for the computation of excited states has only recently been revisited and exploited to compute vertical excitation energies of various small molecules [23, 24]. Different functionals for the optimization of the variance [19, 22, 23] have also been put forward with the common attractive feature of the built-in possibility to target a specific state and avoid in principle the complications encountered in energy minimization where,

without constraints, one would generally collapse to lower-energy states.

For our study, we select two molecules, a small cyanine dye and a retinal model, because of the difficulties they pose in the computation of the lowest vertical excitation energy [4, 25–28], and the different requirements in the procedure adopted in energy minimization: while the ground and excited states of the cyanine belong to different symmetries and can therefore be treated in a state-specific manner, this is not the case for the retinal model, where energy minimization must be performed in a state-average fashion. For both molecules and therefore regardless of the nature of the optimization, we find that energy minimization leads to the stable and fast convergence of the total energies of the states of interest. Furthermore, with the use of compact and balanced energy-minimized wave functions constructed through a selected configuration interaction (CI) approach, we recover vertical excitation energies which are already at the variational Monte Carlo (VMC) level within chemical accuracy (about 0.04 eV) of the reference coupled cluster or extrapolated CI values. On the other hand, for both molecules and for nearly all wave functions investigated, the optimization of all parameters in variance minimization is problematic since it results in the apparent loss of the state of interest over sufficiently long optimization runs, precluding the estimate of the excitation energy. This occurs for the different functionals originally proposed to stabilize the optimization and, surprisingly, in some cases also when targeting the ground state. This finding is unexpected, especially considering that variance minimization has been the method of choice in QMC for decades and is still routinely used, albeit for wave functions with a small number of parameters or where the optimization is limited either to few optimization steps or to the Jastrow factor.

To understand these newly-found issues, we examine how variance minimization behaves when optimizing the linear coefficients of a very simple wave function. Working in the linear sub-space spanned by a few approximate eigenvectors, we

\* w.j.briels@utwente.nl

† moroni@democritos.it

‡ c.filippi@utwente.nl

discover that the optimization of the CI parameters in variance minimization does not converge to the target eigenstate but to a different one: for approximate wave functions, the multiple minima of the variance have generally different values and, during the minimization, the system slowly reaches the eigenstate corresponding to the absolute minimum of the variance, no matter what the starting state is. We show that a similar behavior can be inferred also for more complicated wave functions and, while the process can be slowed down by reducing the statistical error on the gradient of the variance driving the minimization, it severely limits the use of variance minimization for the optimization of realistic wave functions.

In Section II, we recap the equations used for energy and variance optimization, discuss the procedure employed for the state-average case, and introduce the ingredients for a stable version of the Newton method in variance minimization. In Section III, we summarize the computational details and, in Section IV, present the accurate vertical excitation energies obtained in energy minimization and the difficulties encountered in variance minimization for both molecules. We elucidate these findings and conclude in Section V.

## II. METHODS

We briefly introduce below the variance and energy minimization approaches used to optimize the wave functions in variational Monte Carlo. While we employ variance minimization as a state-specific approach to target a given state, we must distinguish between a state-specific and a state-average route for energy optimization when the excited state of interest is of different or equal symmetry, respectively, than other lower-lying states.

### A. Wave function form

The wave functions employed in this work are of the Jastrow-Slater type, namely, the product of a determinantal expansion and a Jastrow correlation function,  $\mathcal{J}$ , as

$$\Psi = \mathcal{J} \sum_{i=1}^{N_{\text{det}}} c_i D_i, \quad (1)$$

where the determinants are expressed on single-particle orbitals and the Jastrow factor includes an explicit dependence on the electron-electron distances. Here, the Jastrow factor is chosen to include electron-electron and electron-nucleus correlation terms [29]. For the determinantal component, we select the relevant determinants according to different recipes: i) very simple ansatzes such as Hartree-Fock (HF) or a CI singles (CIS) expansion recently put forward as a computationally cheap and sufficiently accurate wave function for excited states in QMC [8, 30]; ii) complete-active-space (CAS) expansions where small sets of important active orbitals are manually identified; iii) CI perturbatively selected iteratively (CIPSI) expansions generated to yield automatically balanced multiple states. All expansions are expressed in terms of

spin-adapted configuration state functions (CSF) to reduce the number of variational parameters.

### B. Energy minimization

For state-specific optimization in energy minimization, we employ the stochastic reconfiguration (SR) method [14, 31] in a low-memory conjugate-gradient implementation [14]. Given a starting wave function  $\Psi$  depending on a set of parameters  $\mathbf{p}$ , we denote the derivatives of  $\Psi$  with respect to a parameter  $p_i$  as  $\Psi_i = \partial_i \Psi$ . At every step of the SR optimization, the parameter variations,  $\Delta p_i$ , are computed according to the equation:

$$\bar{\mathbf{S}} \Delta \mathbf{p} = -\frac{\tau}{2} \mathbf{g}, \quad (2)$$

where  $\tau$  is a positive quantity chosen small enough to guarantee the convergence. The vector  $\mathbf{g}$  is the gradient of the energy with components:

$$\begin{aligned} g_i &= \frac{\partial E}{\partial p_i} = 2 \left[ \frac{\langle \Psi_i | \hat{\mathcal{H}} | \Psi \rangle}{\langle \Psi | \Psi \rangle} - E \frac{\langle \Psi | \Psi_i \rangle}{\langle \Psi | \Psi \rangle} \right] \\ &= 2 \left[ \left\langle \frac{\Psi_i}{\Psi} E_L \right\rangle - \langle E_L \rangle \left\langle \frac{\Psi_i}{\Psi} \right\rangle \right], \end{aligned} \quad (3)$$

where  $E_L = \hat{H}\Psi/\Psi$  is the so-called local energy and  $\langle \cdot \rangle$  denotes the Monte Carlo average of the quantity in brackets over the electron configurations sampled from  $\Psi^2 / \langle \Psi | \Psi \rangle$ . The matrix  $\bar{\mathbf{S}}$  has components:

$$\begin{aligned} \bar{S}_{ij} &= \frac{\langle \Psi_i | \Psi_j \rangle}{\langle \Psi | \Psi \rangle} - \frac{\langle \Psi | \Psi_i \rangle \langle \Psi | \Psi_j \rangle}{\langle \Psi | \Psi \rangle^2} \\ &= \left\langle \frac{\Psi_i}{\Psi} \frac{\Psi_j}{\Psi} \right\rangle - \left\langle \frac{\Psi_i}{\Psi} \right\rangle \left\langle \frac{\Psi_j}{\Psi} \right\rangle \equiv \left\langle \frac{\bar{\Psi}_i}{\Psi} \frac{\bar{\Psi}_j}{\Psi} \right\rangle, \end{aligned} \quad (4)$$

which is expressed in the last equality as the overlap matrix in the semi-orthogonal basis,  $\bar{\Psi}_i = \Psi_i - [\langle \Psi | \Psi_i \rangle / \langle \Psi | \Psi \rangle] \Psi$ .

When the state of interest is energetically not the lowest in its symmetry class, we start from a set of wave functions for the multiple states which share the same Jastrow factor and orbitals but are characterized by different linear CI coefficients as

$$\Psi^I = \mathcal{J} \sum_{i=1}^{N_{\text{det}}} c_i^I D_i, \quad (5)$$

where the superscript  $I$  indicates a particular state. To obtain a balanced description of the states of interest, we optimize the non-linear parameters of the orbitals and the Jastrow factor by minimizing the state-average energy [1]:

$$E^{\text{SA}} = \sum_I w_I \frac{\langle \Psi^I | \hat{\mathcal{H}} | \Psi^I \rangle}{\langle \Psi^I | \Psi^I \rangle}, \quad (6)$$

where the weights  $w_I$  are kept fixed and  $\sum_I w_I = 1$ . To this aim, we follow the SR scheme (Eq. 2) and use the gradient of the state-average energy

$$g_i^{\text{SA}} = \sum_I w_I g_i^I, \quad (7)$$

where  $g_i^I$  is the gradient with respect to a parameter  $p_i$  of the energy of state  $I$ , which is computed from the wave function  $\Psi^I$  and its derivatives as in Eq. 3. Moreover, in analogy to the single-state optimization, we introduce a weighted-average overlap matrix defined as

$$\bar{S}_{ij}^{\text{SA}} = \sum_I w_I \bar{S}_{ij}^I, \quad (8)$$

where the overlap matrix for each state is computed from the corresponding wave function as in Eq. 4. We stress that, while the state-average SR procedure is defined simply by analogy with the single-state case, it does lead to the minimization of the state-average energy since we employ the appropriate  $\mathbf{g}^{\text{SA}}$ .

We alternate a number of optimization steps of the non-linear parameters with the optimization of the linear coefficients  $c_i^I$ , whose optimal values are the solution of the generalized eigenvalue equations

$$\mathbf{H}^{\text{CI}} \mathbf{c}^I = E_I \mathbf{S}^{\text{CI}} \mathbf{c}^I, \quad (9)$$

where the Hamiltonian and overlap matrix elements are defined in the basis of the functions  $\{\mathcal{J}D_i\}$  and estimated through Monte Carlo sampling. After diagonalization of Eq. 9, orthogonality between the individual states is automatically enforced. To solve the eigenvalue equation with a memory efficient algorithm, we use the Davidson diagonalization scheme in which the lowest energy eigenvalues are computed without the explicit construction of the entire Hamiltonian and overlap matrices [14]. A similar procedure was recently followed in Ref. [32].

### C. Variance minimization

To perform variance minimization, we can directly minimize the variance of the state of interest,

$$\sigma^2 = \frac{\langle \Psi | (\hat{\mathcal{H}} - E)^2 | \Psi \rangle}{\langle \Psi | \Psi \rangle}, \quad (10)$$

or follow a somewhat more stable optimization procedure by minimizing the expression

$$\sigma_\omega^2 = \frac{\langle \Psi | (\hat{\mathcal{H}} - \omega)^2 | \Psi \rangle}{\langle \Psi | \Psi \rangle}, \quad (11)$$

where the energy  $\omega$  is fixed during the optimization step and then appropriately modified to follow the current value of the energy as originally proposed in Ref. [19]. Recently, a functional  $\Omega$  has been put forward,

$$\Omega = \frac{\langle \Psi | (\omega - \hat{\mathcal{H}}) | \Psi \rangle}{\langle \Psi | (\omega - \hat{\mathcal{H}})^2 | \Psi \rangle}, \quad (12)$$

whose minimization is equivalent to variance minimization if  $\omega$  is eventually updated to the running value of  $E - \sigma$  [23].

Because of its simplicity, we choose here the functional  $\sigma_\omega^2$  but also compare the convergence behavior obtained with the

functional  $\Omega$ . To this aim, we use the Newton optimization method as in Ref. [22] and update the parameters as

$$\Delta \mathbf{p} = -\tau \mathbf{h}^{-1} \mathbf{g}, \quad (13)$$

where  $\mathbf{g}$  is here the gradient of  $\sigma_\omega^2$  and  $\mathbf{h}$  its Hessian matrix, and the parameter  $\tau$  is introduced to damp the size of the variations.

The components of the gradient are given by

$$g_i = 2 \left[ \left\langle \frac{\hat{\mathcal{H}} \Psi_i}{\Psi} E_L \right\rangle - \left\langle \frac{\Psi_i}{\Psi} \right\rangle \langle E_L^2 \rangle - \omega \left( \left\langle \frac{\Psi_i}{\Psi} E_L \right\rangle + \left\langle \frac{\hat{H} \Psi_i}{\Psi} \right\rangle - 2 \left\langle \frac{\Psi_i}{\Psi} \right\rangle \langle E_L \rangle \right) \right], \quad (14)$$

and we discuss other possible equivalent expressions and their relative fluctuations in the SI. The Hessian matrix elements require the second derivatives of the wave function and, to avoid their computation, we follow the same approximation strategy of the Levenberg-Marquardt algorithm [33] and manipulate the expression of the variance in a somewhat different way than proposed in Refs. [20, 22, 34], to obtain the approximate expression of the Hessian matrix

$$h_{ij} = \left\langle \left[ \partial_i E_L + (E_L - \omega) \left( \frac{\Psi_i}{\Psi} - \left\langle \frac{\Psi_i}{\Psi} \right\rangle \right) \right] \times \left[ \partial_j E_L + (E_L - \omega) \left( \frac{\Psi_j}{\Psi} - \left\langle \frac{\Psi_j}{\Psi} \right\rangle \right) \right] \right\rangle, \quad (15)$$

Details of the derivation and alternative expressions for the Hessian are given in the SI.

We use the Newton method and the Hessian  $\mathbf{h}$  (Eq. 15) when optimizing both  $\sigma_\omega^2$  and the  $\Omega$  functional in combination with the corresponding gradient. Furthermore, we follow Ref. [23] in keeping  $\omega$  fixed to an appropriate guess energy for an initial number of minimization steps, upgrading it linearly to the running energy (or  $E - \sigma$  in the case of  $\Omega$ ) over some intermediate iteration steps, and then setting it equal to the current energy estimate for the rest of the run.

### III. COMPUTATIONAL DETAILS

All QMC calculations are carried out with the program package CHAMP [35]. We employ scalar-relativistic energy-consistent HF pseudopotentials and the correlation-consistent Gaussian basis sets specifically constructed for these pseudopotentials [36, 37]. Unless otherwise specified, we use a double- $\zeta$  basis set minimally augmented with  $s$  and  $p$  diffuse functions on the heavy atoms and denoted here as maug-cc-pVDZ. Basis-set convergence tests are performed with the fully augmented double (aug-cc-pvDZ) and triple (aug-cc-pvTZ) basis sets. In all cases, the exponents of the diffuse functions are taken from the corresponding all-electron Dunning's correlation-consistent basis sets [38].

In the state-specific (energy and variance) optimization runs, we sample a guiding wave function that differs from

the current wave function close to the nodes [39] to guarantee finite variances of the estimators of the gradient, overlap, and Hessian matrix elements. In the state-average energy minimizations, we employ equal weights for the multiple states and sample a guiding wave function constructed as  $\Psi_g^2 = \sum_I |\Psi^I|^2$ , to ensure that the distribution sampled has a large overlap with all states of interest [1]. All wave function parameters (Jastrow, orbital, and CI coefficients) are optimized and the damping factor,  $\tau$ , in the SR and the Newton method is set to 0.05 and 0.1, respectively, unless otherwise specified. In the DMC calculations, we treat the pseudopotentials beyond the locality approximation using the T-move algorithm [40] and employ an imaginary time-step of 0.05 a.u. which yields excitation energies converged to better than 0.01 eV as shown in the SI.

The HF, CIS, and complete-active-space self-consistent-field (CASSCF) calculations are carried out with the program GAMESS(US) [41, 42]. For the cyanine dye, we consider different CAS expansions: a CAS(6,5) and CAS(6,10) correlating 6  $\pi$  electrons in the orbitals constructed from the  $2p_z$  and  $3p_z$  atomic orbitals; a truncated CAS(14,13) consisting of 6  $\pi$  and 8  $\sigma$  electrons in 13 bonding and antibonding orbitals. For the retinal model, we employ a minimal CAS(6,6) active space of 6  $\pi$  electrons in the orbitals constructed from the  $2p_z$  atomic orbitals.

The CIPSI calculations are performed with Quantum Package [43] and the determinantal expansions are constructed to be eigenstates of  $\hat{S}^2$ . For the cyanine dye where ground and excited states have different symmetry, we follow two paths to construct the CIPSI expansions: i) we perform separate expansions for the two states starting from the corresponding CASSCF(6,10) orbitals, and match the variances of the CI wave functions to obtain a balanced description of the states. We find that this procedure leads to an automatic match of the second-order perturbation theory (PT2) energy contributions as shown in Table S1. ii) We perform the expansion of the two states simultaneously, using a common set of orbitals (the excited-state CASSCF(6,10) orbitals), and obtain automatically matched PT2 energy corrections during the expansion [9]. For the retinal model where the ground and excited states have the same symmetry, we have only one set of orbitals for the CIPSI expansions. In this case, we perform a simultaneous expansion with a selection scheme that matches the CI variances and also attempts to balance the PT2 energy contributions of the two states (see SI) [44].

All total energies are computed on the PBE0/cc-pVQZ ground-state geometry of the cyanine [45] and retinal molecules. The DFT geometry optimization of the retinal model is performed with the program Gaussian [46]. The coupled cluster results are obtained with Psi4 [47].

#### IV. RESULTS

We compute the lowest  $\pi \rightarrow \pi^*$  vertical excitation energy of the cyanine dye ( $C_3H_3(NH_2)_2^+$ ) and the minimal model of the retinal protonated Schiff base ( $C_5H_6NH_2^+$ ) depicted in Fig. 1 and denoted as CN5 and PSB3, respectively. As already

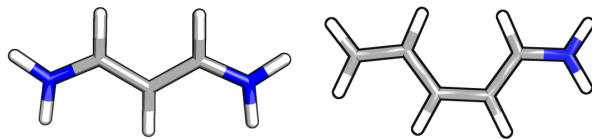


FIG. 1. Schematic representations of the CN5 (left) and PSB3 (right) molecules. White, gray, and blue denote hydrogen, carbon, and nitrogen, respectively.

mentioned, while being generally challenging for electronic structure methods [4, 25–28], these examples are representative of the two cases of a ground ( $S_0$ ) and an excited ( $S_1$ ) state of different (CN5) and equal (PSB3) symmetry. Correspondingly, the energy minimization scheme is state-specific for CN5 and state-average for PSB3, while variance minimization affords a state-specific optimization for both molecules, at least in principle.

#### Ground and excited states of different symmetry

In Table I, we list the ground- and excited-state energies, and corresponding excitation energies of CN5 computed in VMC and DMC with different wave functions optimized by (state-specific) energy minimization. The simplest case consists of a single determinant (HF) and a HOMO-LUMO (HL) two-determinant wave function for the ground and the excited state, respectively. We then consider configuration interaction singles (CIS) expansions, CAS expansions with increasing active spaces, and balanced CIPSI expansions with different choices of the starting orbitals, namely, independent sets for the two states (CIPSI-SS) or a common set of orbitals (CIPSI- $B_1$ ). The excitation energies are displayed in Fig. 2.

The general trend is a decrease of the excitation energy towards the extrapolated full CI (exFCI) and approximate coupled cluster singles, doubles and triples model (CC3) reference values for better wave functions. As an exception, when we move from the HF/HL to CIS wave functions, the VMC energies of both states decrease but the corresponding excitation energy becomes worse. With increasingly large CAS expansions, both the total and the excitation energies improve but the convergence is very slow. For all these wave functions, the DMC excitation energy is lower than the VMC value and becomes within 0.1 eV of the reference results for the largest active spaces with about 50,000 and 70,000 determinants for the ground and the excited state, respectively. By comparison, the errors of TDDFT and CASPT2 can be as large as 0.4 and  $-0.2$  eV, respectively [4, 45].

The quality of the results exhibits a further, dramatic improvement with the use of CIPSI expansions. The VMC and DMC energies obtained with the smallest CIPSI wave function are lower than the corresponding values obtained with the largest CAS considered here. Furthermore, constructing ground- and excited-state CIPSI expansions with similar PT2 corrections leads to a balanced description of both states and to VMC excitation energies which change very little with increasing expansion size, being irregularly scattered over a

TABLE I. VMC and DMC total energies (a.u.) and excitation energies ( $\Delta E$ , eV) of CN5 obtained for different wave functions optimizing all parameters (Jastrow, orbital, and CI coefficients) in energy minimization.

WF	No. det		No. parm		$E_{\text{VMC}}$		$\Delta E_{\text{VMC}}$	$E_{\text{DMC}}$		$\Delta E_{\text{DMC}}$
	S0	S1	S0	S1	S0	S1		S0	S1	
HF/HL	1	2	516	529	-40.8372(4)	-40.6460(3)	5.202(14)	-40.9378(3)	-40.7509(3)	5.086(11)
HF/CIS	1	980	516	4751	-40.8372(4)	-40.6505(3)	5.080(14)	-40.9378(3)	-40.7533(3)	5.020(11)
CIS	999	980	5260	4751	-40.8444(4)	-40.6505(3)	5.278(14)	-40.9393(3)	-40.7533(3)	5.061(11)
CAS(6,5)	52	48	567	561	-40.8468(4)	-40.6583(4)	5.130(15)	-40.9433(3)	-40.7582(2)	5.038(10)
CAS(6,10)	7232	7168	3134	3064	-40.8498(4)	-40.6628(4)	5.090(15)	-40.9439(3)	-40.7594(3)	5.022(11)
CAS(14,13)	48206	72732	9480	11727	-40.8583(3)	-40.6713(3)	5.091(10)	-40.9442(7)	-40.7611(7)	4.983(26)
CIPSI-SS	376	1094	1567	2609	-40.8646(3)	-40.6842(3)	4.908(12)	-40.9467(3)	-40.7665(3)	4.905(10)
	1344	4382	2478	4531	-40.8798(3)	-40.7013(3)	4.857(13)	-40.9502(2)	-40.7711(2)	4.872(09)
	2460	8782	3555	6561	-40.8896(3)	-40.7099(3)	4.890(12)	-40.9532(2)	-40.7748(2)	4.856(09)
	3913	14114	4842	8312	-40.8941(2)	-40.7167(3)	4.828(11)	-40.9559(2)	-40.7775(2)	4.856(08)
CIPSI-B <sub>1</sub>	2456	6120	3971	5466	-40.8847(2)	-40.7053(2)	4.880(09)	-40.9521(2)	-40.7727(2)	4.881(09)
	4829	13130	5737	8021	-40.8945(3)	-40.7150(3)	4.889(13)	-40.9560(2)	-40.7766(2)	4.882(08)
exFCI/aug-cc-pVDZ [48]										4.89
CC3/aug-cc-pVDZ										4.851
CC3/aug-cc-pVTZ										4.844

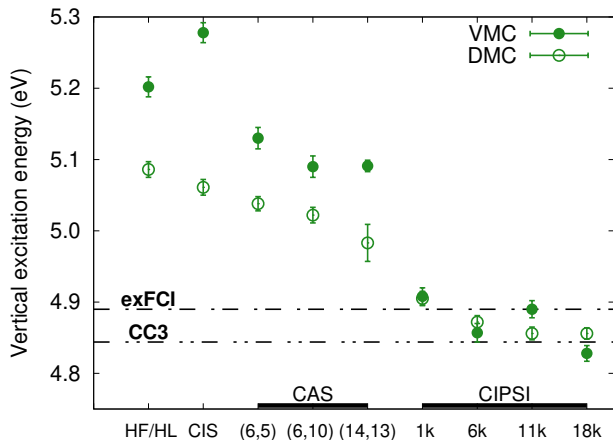


FIG. 2. VMC and DMC excitation energies of CN5 calculated with different wave functions optimized in energy minimization. The exFCI/aug-cc-pVDZ [48] and CC3/aug-cc-pVTZ reference values are also shown. The approximate total number of determinants for the CIPSI-SS wave functions of the ground and excited states is indicated.

small energy range of 0.08 eV. Importantly, the DMC excitation energies are compatible with the VMC ones and in excellent agreement with the CC3 and exFCI values. Finally, employing two different sets of orbitals to generate the CIPSI expansions leads to marginal differences, namely, to DMC excitation energies of 4.856(8) and 4.882(8) eV, which are both bracketed by the reference values.

Having verified that state-specific energy optimization in combination with accurate wave functions allows the robust treatment of CN5, we now employ variance minimization with the  $\sigma_{\omega}^2$  functional to optimize the CAS(6,5) and

CAS(6,10) wave functions of the ground and excited states. The convergence of the corresponding VMC variances and energies is shown in Fig. 3. For the smaller CAS(6,5), we observe that, while the variance converges rather quickly, the energy appears to do so more slowly and only after undershooting to a value which generally depends on the statistical error and initial conditions of the run. As reported in Table II, the optimal ground- and excited-state energies are higher by about 30 mHartree than the corresponding values obtained in energy minimization but the resulting excitation energy is compatible within statistical error.

If we move to the larger CAS(6,10) determinantal expansion, we find however that, while the variance reaches a stable value and the ground-state energy has a similar behavior to the CAS(6,5) case, the energy of the excited state grows steadily and it is therefore not possible to estimate the vertical excitation energy of the system. Surprisingly, even in the simplest case of the one-configuration (HF/HL) wave functions, the energy of the excited state keeps slowly rising even after 600 iterations as shown in Fig. 4, while the ground-state energy behaves similarly to the corresponding CAS cases.

We stress that, for most wave functions of Table I, we observe a steady growth of the excited-state energy in variance minimization and, therefore, wonder whether optimizations which appear converged are not simply affected by a much slower drift in the energy, which would become evident only in longer runs. Importantly, the apparently unstable behavior is independent of the initial value of  $\omega$  and the number of steps over which we keep  $\omega$  fixed (see Section S6). The use of a smaller or larger damping factors (i.e.  $\tau = 0.04$  and 0.2) leads to the same pathological growth of the excited-state energy, characterized by the same slope as a function of time as shown in Fig. S4. Moreover, we recover the same behavior also when using a gradient-only-based optimizer (see Fig. S7).

TABLE II. VMC energies and variances (a.u.) and vertical excitation energies (eV) of CN5 obtained with energy and variance minimization.

	Energy min.					Variance min.				
	E(S0)	E(S1)	$\Delta E$	$\sigma^2(S0)$	$\sigma^2(S1)$	E(S0)	E(S1)	$\Delta E$	$\sigma^2(S0)$	$\sigma^2(S1)$
CAS(6,5)	-40.8468(4)	-40.6583(4)	5.13(1)	0.928	0.940	-40.8170(5)	-40.6270(5)	5.17(2)	0.856	0.862
CAS(6,10)	-40.8498(4)	-40.6628(4)	5.09(1)	0.928	0.930	-40.8163(4)	—	—	0.855	—

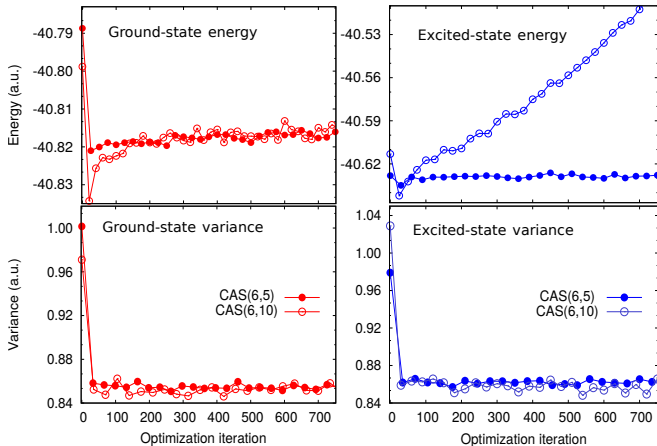
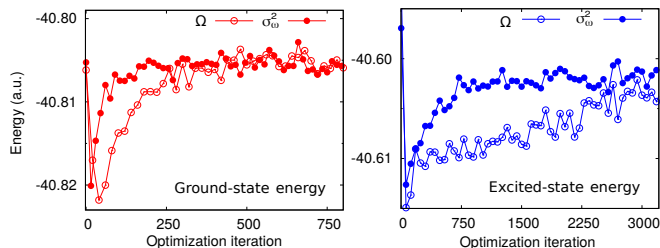


FIG. 3. Convergence of the VMC energy (top) and variance (bottom) of the ground (left) and excited (right) states of CN5 in the optimization of the CAS(6,5) and CAS(6,10) wave functions in variance minimization.

Finally, minimizing the  $\Omega$  functional instead of  $\sigma_\omega^2$  yields an excited-state energy which ultimately rises with iterations as shown for the excited-state HL wave function in Fig. 4.

FIG. 4. Convergence of VMC energy of the ground (left) and excited (right) states of CN5 in the optimization of the HF/HL wave functions within variance minimization with the  $\sigma_\omega^2$  (our default) and the  $\Omega$  functional.

### Ground and excited states of the same symmetry

For PSB3, we optimize the wave functions in energy minimization in a state-average fashion and report the resulting VMC and DMC total energies and vertical excitation energies in Table III. As in the CN5 case, CIPSI wave functions are superior to CAS expansions of similar size and, with only about 400 determinants, the use of CIPSI yields not only lower total energies but also a VMC vertical excitation energy in good

agreement with the CC3 reference, largely correcting the error of 0.25 eV obtained with the CAS(6,6) wave function. For all CIPSI expansions, the DMC excitation energies are always quite close to the correspondent VMC results and, for the larger expansions, within 0.05 eV of the CC3 value.

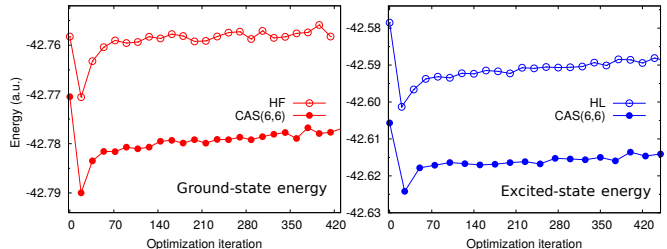


FIG. 5. Convergence of the VMC energy of the ground (red) and excited (blue) states of PSB3 in the optimization of the RHF/HL and CAS(6,6) wave functions within variance minimization.

When we perform state-specific variance minimization, we encounter great difficulties in the convergence of the energies as we show for the HF/HL and CAS(6,6) wave functions in Fig. 5. Differently from CN5, we find in general that not only the energy of the excited state but also that of the ground state grows steadily with iteration number. We only obtain a seemingly stable energy for the HF wave function.

## V. DISCUSSION AND CONCLUSIONS

While our results confirm the high accuracy reachable in QMC with energy minimization, they evidence severe problems in variance minimization which, in most cases, preclude the estimation of the excitation energy. To gain a better understanding of the troublesome behavior of the energy during variance minimization, we further investigate the simple case of the HL wave function of CN5 (Fig. 4) and find that the energy of the state drifts to higher values during variance minimization also when one optimizes only the LUMO orbital. Therefore, since optimization of an orbital can be achieved by mixing it with the unoccupied ones of the same symmetry, we can recast the LUMO optimization into the linear variation of the CI coefficients of the single excitations out of the LUMO orbital, which amount to only twelve additional CSFs in our basis set. With such a small expansion, we can then diagonalize the Hamiltonian in the basis of the CSFs times the Jastrow factor to estimate its thirteen eigenvalues and eigenvectors, and work directly in the basis of the eigenstates to assess the behavior of variance minimization when starting from the states which are optimal for energy minimization.



TABLE III. VMC and DMC total energies (a.u.) and vertical excitation energies (eV) of PSB3 obtained with different wave functions optimized in energy minimization.

WF	No. det	No. param	VMC			DMC		
			E(S0)	E(S1)	$\Delta E$	E(S0)	E(S1)	$\Delta E$
CAS(6,6)	400	1645	-42.8091(2)	-42.6471(2)	4.409(9)	-42.9118(2)	-42.7541(2)	4.293(6)
CIPSI	422	4011	-42.8174(2)	-42.6623(2)	4.221(9)	-42.9133(2)	-42.7578(2)	4.233(6)
	1158	5968	-42.8297(2)	-42.6735(2)	4.252(9)	-42.9160(2)	-42.7609(2)	4.221(6)
	2579	8106	-42.8357(2)	-42.6796(2)	4.247(9)	-42.9169(2)	-42.7621(2)	4.214(6)
CC3/aug-cc-pVDZ								4.19
CC3/aug-cc-pVTZ								4.16

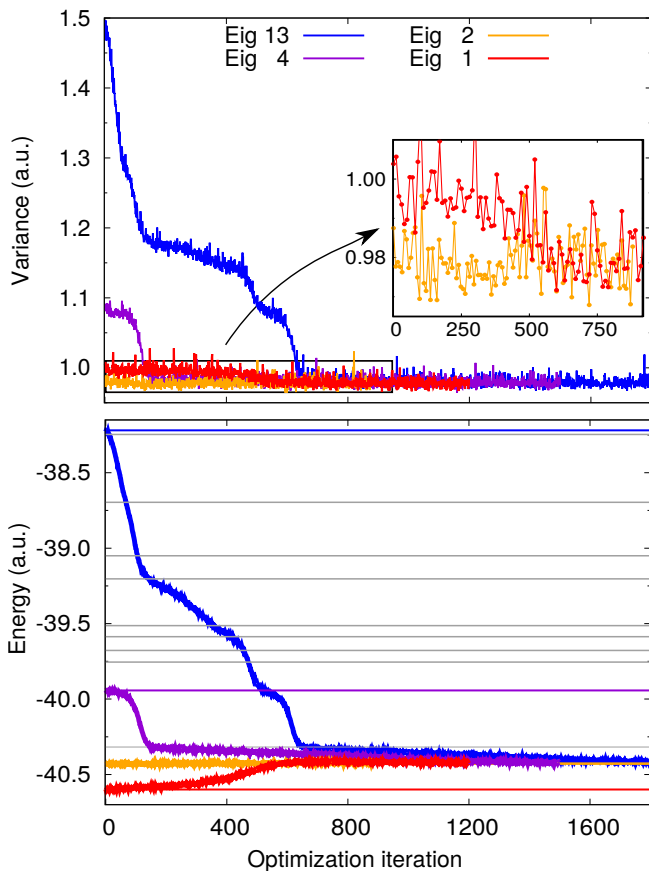


FIG. 6. Convergence of the VMC variance (top) and energy (bottom) of CN5 in the CI optimization of a small expansion (see text) with variance minimization. The horizontal lines in the energy plot correspond to the eigenvalues in this reduced space, and the colored ones are the eigenstates used as starting point in four optimization runs. The damping factor used in the Newton method is  $\tau = 0.2$ .

In Fig. 6, we show the evolution of the VMC variance and energy for four variance minimization runs in which we start from different eigenvectors, taking the corresponding eigenvalues as initial target energies  $\omega$ . In particular, we consider the lowest state in  $B_1$  symmetry as well as the second, fourth, and thirteenth (corresponding to the highest energy) states. We note that, since our states are not exact eigenstates of the

full Hamiltonian, the corresponding variances of the local energy are non zero and are spread over about 0.5 a.u. with the lowest value in correspondence of the second state. In principle, one would expect to find a feature of the variance landscape—ideally a local minimum—near each of the approximate eigenstates since the functionals  $\sigma_\omega^2$  or  $\Omega$  are designed to select a particular state through the initial value of  $\omega$ , and minimize the variance of *that* state. Here, the selection of the state is further facilitated starting each run precisely from the chosen eigenstate, and variance minimization should perform minor adjustments of the initial parameters from their optimal values for the energy.

The behavior illustrated in Figs. 6 is totally different, with all optimization runs leaking down to successive lower-variance states and eventually converging to the absolute minimum corresponding to the second eigenstate. The staircase shape of the variance evolution points to the presence of flat regions of the variance landscape close to the eigenstates, from which the optimization can eventually escape. This is further corroborated if we follow the evolution of the CI coefficients as shown starting from the highest-energy state in Fig. 7: the initial coefficient quickly decreases to zero and other eigenstates become populated until convergence on the second state. In proximity of some eigenstates, the variance displays a more pronounced plateau, where the system spends enough time to acquire the full character of that particular state. It is also interesting to note that the states are populated sequentially with the order determined by decreasing energies. We stress that we observe a similar behavior of the variance also when using the  $\Omega$  functional starting from the same set of approximate eigenstates (see Fig. S8).

In Fig. 8, we investigate the impact of the statistical error on the loss of the selected state. In particular, we focus on the evolution of the variance and the energy starting from the 4<sup>th</sup> eigenvector for different lengths of the VMC runs used to compute the gradient and Hessian matrix. The shortest run (larger statistical error) loses the target state in a slightly smaller number of steps. However the intermediate and the longest run give very similar results, suggesting that even longer VMC runs would not stabilize the target state.

Finally, to verify that the understanding gained here also applies to more complicated wave functions, we revisit the very problematic optimization of the excited-state CAS(6,10) wave function (Fig. 3) and perform a much longer calculation, finding that the energy eventually converges as shown in

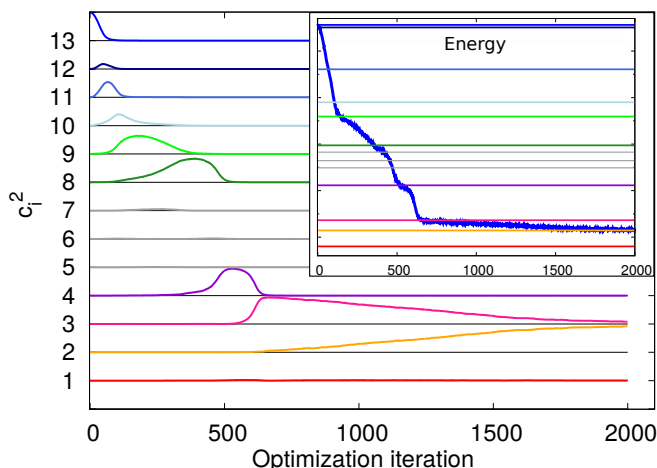


FIG. 7. Evolution of the square of the CI coefficients  $c_i^2$  (offset by  $i$  for clarity) of the small expansion of CN5 during variance minimization, for the run starting from the 13<sup>th</sup> eigenvector; in the inset, the evolution of the energy is replicated to emphasize flat regions in the energy landscape close to an eigenstate (i.e. when the corresponding  $c_i \sim 1$ ).

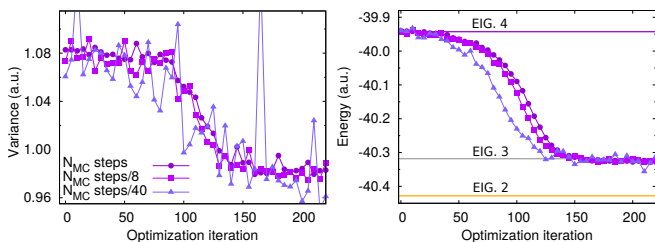


FIG. 8. Convergence of the variance (left) and energy (right) for different lengths of the Monte Carlo runs used to compute the gradient and Hessian matrix during the optimization, starting from the 4<sup>th</sup> eigenvector.  $N_{MC}$  is the number of Monte Carlo steps used in Fig. 6.

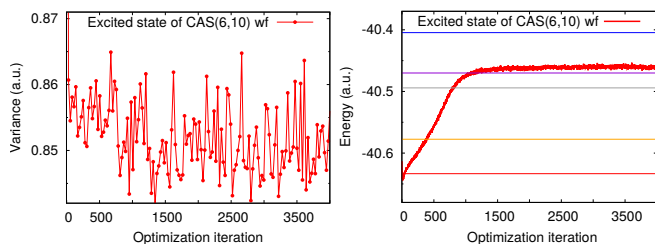


FIG. 9. Variance (left) and energy (right) convergence for the optimization of the excited state of the CAS(6,10) wave function. The horizontal lines in the energy plot correspond to the firsts eigenvalue roots obtained with the Davidson optimization.

Fig. 9. For the final set of Jastrow and orbital parameters, we determine the eigenvalues in the linear space of the determinants times the Jastrow factor and recover a similar behavior to what observed in the simple example: the minimization of  $\sigma_\omega^2$  brings the system approximately to an eigenstate with a lower variance, which is in this case the 4<sup>th</sup> one.

In summary, we have shown that the combination of energy minimization with an appropriate choice of the ground- and excited-state wave functions via a balanced CIPSI procedure leads to excitation energies that are in excellent agreement already at the VMC level with the reference values. In particular, we obtained a robust convergence of the total ground- and excited-state energies, and a very accurate excitation energy not only in the easier state-specific case of CN5 but also when employing energy minimization in a state-average fashion for PSB3. On the other hand, we encountered severe problems when employing variance minimization since, over sufficiently long optimization runs, one may loose the state of interest in favor of a state with lower variance, as we clearly demonstrated with a simple but realistic example. Even though, theoretically, the functionals  $\sigma_\omega^2$  and  $\Omega$  have a built-in possibility to target the energy of a specific state, in practice, this is generally not sufficient to maintain the parameters close to the desired local minimum of the variance. Therefore, these considerations lead to the conclusion that, with the present functionals and no *a priori* knowledge of the parameter landscape of the variance for the system of interest, energy minimization is a safer and more stable procedure.

## ACKNOWLEDGMENT

A.C. is supported by the ‘‘Computational Science for Energy Research and Netherlands eScience Center joint program’’ (project CSER.JCER.022) of the Netherlands Organisation for Scientific Research (NWO). This work was carried out on the Dutch national supercomputer Cartesius with the support of SURF Cooperative.

## CONTENT OF SI

Derivation and discussion of the expressions of the gradient and approximate Hessian of the variance; CIPSI energies for various expansions; basis-set dependence of the VMC and DMC excitation energies; DMC excitation energy versus time step; dependence of variance minimization on the choice of  $\omega$ , number of steps with  $\omega$  fixed, damping factor in the Newton method, and statistical error; optimizations with a gradient-based optimizer and with the  $\Omega$  functional.

[1] C. Filippi, M. Zaccheddu, and F. Buda, *J. Chem. Theory Comput.* **5**, 2074 (2009).  
 [2] P. M. Zimmerman, J. Toulouse, Z. Zhang, C. B. Musgrave, and C. Umrigar, *J. Chem. Phys.* **131**, 124103 (2009).

[3] O. Valsson and C. Filippi, *J. Chem. Theory Comput.* **6**, 1275 (2010).  
 [4] R. Send, O. Valsson, and C. Filippi, *Journal of Chemical Theory and Computation* **7**, 444 (2011).



- [5] O. Valsson, P. Campomanes, I. Tavernelli, U. Rothlisberger, and C. Filippi, *J. Chem. Theory Comput.* **9**, 2441 (2013).
- [6] R. Guareschi, H. Zufikri, C. Daday, F. M. Floris, C. Amovilli, B. Mennucci, and C. Filippi, *Journal of Chemical Theory and Computation* **12**, 1674 (2016).
- [7] R. J. Hunt, M. Szyniszewski, G. I. Prayogo, R. Maezono, and N. D. Drummond, *Phys. Rev. B* **98**, 075122 (2018).
- [8] N. S. Blunt and E. Neuscamman, *J. Chem. Theory Comput.* **15**, 178 (2019).
- [9] M. Dash, J. Feldt, S. Moroni, A. Scemama, and C. Filippi, *J. Chem. Theory Comput.* **15**, 4896 (2019).
- [10] W. M. C. Foulkes, L. Mitas, R. J. Needs, and G. Rajagopal, *Reviews of Modern Physics* **73**, 33 (2001).
- [11] A. Lüchow, *Wiley Interdisciplinary Reviews: Computational Molecular Science* **1**, 388 (2011).
- [12] B. M. Austin, D. Y. Zubarev, and W. A. Lester, *Chemical Reviews* **112**, 263 (2012).
- [13] S. Sorella and L. Capriotti, *The Journal of Chemical Physics* **133**, 234111 (2010).
- [14] E. Neuscamman, C. J. Umrigar, and G. K.-L. Chan, *Phys. Rev. B* **85**, 045103 (2012).
- [15] C. Filippi, R. Assaraf, and S. Moroni, *J. Chem. Phys.* **144**, 194105 (2016).
- [16] R. Assaraf, S. Moroni, and C. Filippi, *J. Chem. Theory Comput.* **13**, 5273 (2017).
- [17] M. Dash, S. Moroni, A. Scemama, and C. Filippi, *J. Chem. Theory Comput.* **14**, 4176 (2018).
- [18] R. L. Coldwell, *International Journal of Quantum Chemistry* **12**, 215 (1977).
- [19] C. J. Umrigar, K. G. Wilson, and J. W. Wilkins, *Phys. Rev. Lett.* **60**, 1719 (1988).
- [20] A. Malatesta, S. Fahy, and G. B. Bachelet, *Phys. Rev. B* **56**, 12201 (1997).
- [21] P. R. C. Kent, R. J. Needs, and G. Rajagopal, *Phys. Rev. B* **59**, 12344 (1999).
- [22] C. J. Umrigar and C. Filippi, *Phys. Rev. Lett.* **94**, 150201 (2005).
- [23] J. A. R. Shea and E. Neuscamman, *Journal of Chemical Theory and Computation* **13**, 6078 (2017).
- [24] S. D. Pineda Flores and E. Neuscamman, *J. Phys. Chem. A* **123**, 1487 (2019).
- [25] O. Valsson, C. Angeli, and C. Filippi, *Phys. Chem. Chem. Phys.* **14**, 11015 (2012).
- [26] M. Huix-Rotllant, M. Filatov, S. Gozem, I. Schapiro, M. Olivucci, and N. Ferré, *Journal of Chemical Theory and Computation* **9**, 3917 (2013).
- [27] D. Tuna, D. Lefrancois, L. Wolański, S. Gozem, I. Schapiro, T. Andruniów, A. Dreuw, and M. Olivucci, *Journal of Chemical Theory and Computation* **11**, 5758 (2015).
- [28] B. Le Guennic and D. Jacquemin, *Accounts of Chemical Research* **48**, 530 (2015).
- [29] As Jastrow factor, we use the exponential of the sum of two fifth-order polynomials of the electron-nuclear and the electron-electron distances, respectively, and rescale the inter-particle distances as  $R = (1 - \exp(-\kappa r))/\kappa$  with  $\kappa$  set to 0.6 a.u. We employ different electron-nucleus Jastrow factors to describe the correlation of an electron with C and H. The total number of free parameters to be optimized in the Jastrow factor is 17 for the systems considered here.
- [30] E. Neuscamman, *The Journal of Chemical Physics* **145**, 081103 (2016).
- [31] S. Sorella, M. Casula, and D. Rocca, *J. Chem. Phys.* **127**, 014105 (2007).
- [32] I. Sabzevari, A. Mahajan, and S. Sharma, *The Journal of Chemical Physics* **152**, 024111 (2020).
- [33] W. T. V. William H. Press, Saul A. Teukolsky and B. P. Flannery, *Numerical Recipes Third Edition* (Cambridge University Press, The Edinburgh Building, Cambridge CB2 8RU, UK, 2007).
- [34] J. Toulouse and C. J. Umrigar, *The Journal of Chemical Physics* **128**, 174101 (2008).
- [35] CHAMP is a quantum Monte Carlo program package written by C. J. Umrigar, C. Filippi, S. Moroni and collaborators.
- [36] M. Burkatzki, C. Filippi, and M. Dolg, *J. Chem. Phys.* **126**, 234105 (2007).
- [37] For the hydrogen atom, we use a more accurate BFD pseudopotential and basis set. Dolg, M.; Filippi, C., private communication.
- [38] R. A. Kendall, T. H. Dunning Jr, and R. J. Harrison, *J. Chem. Phys.* **96**, 6796 (1992).
- [39] C. Attaccalite and S. Sorella, *Phys. Rev. Lett.* **100**, 114501 (2008).
- [40] M. Casula, *Phys. Rev. B* **74**, 161102 (2006).
- [41] M. W. Schmidt, K. K. Baldridge, J. A. Boatz, S. T. Elbert, M. S. Gordon, J. H. Jensen, S. Koseki, N. Matsunaga, K. A. Nguyen, S. Su, and others, *J. Comput. Chem.* **14**, 1347 (1993).
- [42] M. S. Gordon and M. W. Schmidt, in *Theory and applications of computational chemistry* (Elsevier, 2005) pp. 1167–1189.
- [43] Y. Garniron, T. Applencourt, K. Gasperich, A. Benali, A. Ferté, J. Paquier, B. Pradines, R. Assaraf, P. Reinhardt, J. Toulouse, P. Barbaresco, N. Renon, G. David, J.-P. Malrieu, M. Vénil, M. Caffarel, P.-F. Loos, E. Giner, and A. Scemama, *Journal of Chemical Theory and Computation* **15**, 3591 (2019).
- [44] Dash, M.; Scemama, A., private communication.
- [45] P. Boulanger, D. Jacquemin, I. Duchemin, and X. Blase, *J. Chem. Theory Comput.* **10**, 1212 (2014).
- [46] M. J. Frisch, G. W. Trucks, H. B. Schlegel, G. E. Scuseria, M. A. Robb, J. R. Cheeseman, G. Scalmani, V. Barone, G. A. Petersson, H. Nakatsuji, X. Li, M. Caricato, A. Marenich, J. Bloino, B. G. Janesko, R. Gomperts, B. Mennucci, H. P. Hratchian, J. V. Ortiz, A. F. Izmaylov, J. L. Sonnenberg, D. Williams-Young, F. Ding, F. Lipparini, F. Egidi, J. Goings, B. Peng, A. Petrone, T. Henderson, D. Ranasinghe, V. G. Zakrzewski, J. Gao, N. Rega, G. Zheng, W. Liang, M. Hada, M. Ehara, K. Toyota, R. Fukuda, J. Hasegawa, M. Ishida, T. Nakajima, Y. Honda, O. Kitao, H. Nakai, T. Vreven, K. Throssell, J. A. Montgomery, J. J. E. Peralta, F. Ogliaro, M. Bearpark, J. J. Heyd, E. Brothers, K. N. Kudin, V. N. Staroverov, T. Keith, R. Kobayashi, J. Normand, K. Raghavachari, A. Rendell, J. C. Burant, S. S. Iyengar, J. Tomasi, M. Cossi, J. M. Millam, M. Klene, C. Adamo, R. Cammi, J. W. Ochterski, R. L. Martin, K. Morokuma, O. Farkas, J. B. Foresman, and D. J. Fox., “Gaussian09, revision a.02; gaussian, inc., wallingford ct,” (2016).
- [47] R. M. Parrish, L. A. Burns, D. G. Smith, A. C. Simmonett, A. E. DePrince III, E. G. Hohenstein, U. Bozkaya, A. Y. Sokolov, R. Di Remigio, R. M. Richard, and others, *J. Chem. Theory Comput.* **13**, 3185 (2017).
- [48] Y. Garniron, A. Scemama, E. Giner, M. Caffarel, and P.-F. Loos, *The Journal of Chemical Physics* **149**, 064103 (2018).